Article

Inorganic Chemistry

The Influence of Phosphorus Substituents on the Structures and Solution Speciation of Trivalent Uranium and Lanthanide **Phosphinodiboranates**

Joshua C. Zgrabik, Rina Bhowmick, Francesca D. Eckstrom, A. Rayford Harrison, Taylor V. Fetrow, Anastasia V. Blake, Bess Vlaisavljevich,* and Scott R. Daly*



Cite This: https://doi.org/10.1021/acs.inorgchem.3c02773



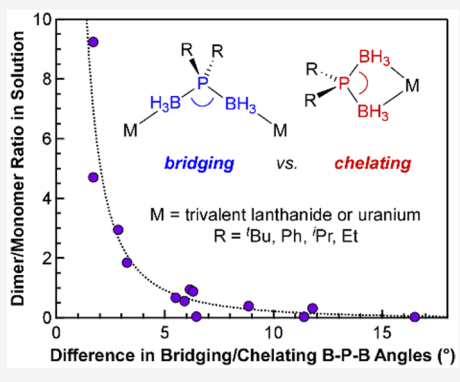
ACCESS I

III Metrics & More

Article Recommendations

Supporting Information

ABSTRACT: Here, we report the mechanochemical synthesis and characterization of homoleptic uranium and lanthanide phosphinodiboranates with isopropyl and ethyl substituents attached to phosphorus. $M(H_3BP^iPr_2BH_3)_3$ complexes with M = U, Nd, Sm, Tb, and Er were prepared by ball milling UI₃(THF)₄, SmBr₃, or MI₃ with three equivalents of $K(H_3BP^iPr_2BH_3)$. $M(H_3BPEt_2BH_3)_3$ with M=U and Nd were prepared similarly using K(H₃BPEt₂BH₃), and the complexes were purified by extraction and crystallization from Et₂O or CH₂Cl₂. Single-crystal XRD studies revealed that all five M(H₃BPⁱPr₂BH₃)₃ crystallize as dimers, despite the significant differences in metal radii across the series. In contrast, Nd(H₃BPEt₂BH₃)₃ with smaller ethyl substituents crystallized as a coordination polymer. Crystals of U(H₃BPEt₂BH₃)₃ were not suitable for structural analysis, but crystals of U(H₃BPMe₂BH₃)₃ isolated in low yield by solution methods were isostructural with Nd(H₃BPEt₂BH₃)₃. ¹H and ¹¹B NMR studies in C₆D₆ revealed that all of the



complexes form mixtures of monomer and oligomers when dissolved, and the extent of oligomerization was highly dependent on metal radius and phosphorus substituent size. A comprehensive analysis of all structurally characterized uranium and lanthanide phosphinodiboranate complexes reported to date, including those with larger Ph and ^tBu substituents, revealed that the degree of oligomerization in solution can be correlated to differences in B-P-B angles obtained from single-crystal XRD studies. Density functional theory calculations, which included structural optimizations in combination with conformational searches using tight binding methods, replicated the general experimental trends and revealed free energy differences that account for the different solution and solid-state structures. Collectively, these results reveal how steric changes to phosphorus substituents significantly removed from metal coordination sites can have a significant influence on solution speciation, deoligomerization energies, and the solid-state structure of homoleptic phosphinodiboranate complexes containing trivalent f-metals.

■ INTRODUCTION

Phosphinodiboranates are monoanionic borohydrides that have the general formula H₃BPR₂BH₃⁻ (abbreviated here as R-PDB, where R is the substituent attached to phosphorus;

Despite being known to form salts with alkali metals with different substituents attached to phosphorus since at least the 1960s, 1-11 and likely as early as 1940, 12 the coordinative properties of phosphinodiboranates with different metals have only emerged recently.¹³ In 2018, we showed that M- $(H_3BP^tBu_2BH_3)_3$ $(M^{-t}Bu)$, where M = uranium or a lanthanide, can be prepared by salt metathesis reactions using trivalent f-metal iodides and K(H₃BP^tBu₂BH₃) (Scheme 2a). 14 Later, in 2021, Morris et al. reported the first magnesium complex containing Ph-PDB. ¹⁵ The β -diketoiminate-supported complex $[(BDI)Mg(H_3BPPh_2BH_3)]_2$ where BDI = HC[C- $(CH_3)Ndipp]_2$ and $dipp = 2.6^{-i}Pr_2C_6H_3$ was prepared by treating the phosphidoborane complex [(BDI)Mg- $(H_3BPPh_2)]_2$ with 2 equiv of $HPPh_2 \cdot BH_3$ (Scheme 2b).

Scheme 1. General Synthesis and Structure of Phosphinodiboranates (Which Are Also Referred to As Phosphido-Bis(borane) Anions)

$$\begin{bmatrix} H_3 & & & \\ H_3 & & & \\ & & & \end{bmatrix}^{1-} \xrightarrow{BH_3 \cdot L} \begin{bmatrix} H_3 & & \\ &$$

Incidentally, similar borane transfer reactivity was implicated in the formation of $U(H_3BP^tBu_2BH_3)_3$ from reactions of $UI_3(1,4-$

Special Issue: Ligand-Metal Complementarity in Rare Earth and Actinide Chemistry

Received: August 9, 2023 Revised: November 2, 2023 Accepted: November 3, 2023



Scheme 2. (a) Initial Salt Metathesis Reactions Used to Prepare M-^tBu with M = U, Nd, and Er; ¹⁴ (b) Synthesis of [(BDI)Mg(H₃BPPh₂BH₃)]₂ via Borane Transfer to the Phosphidoborane Ligand in [(BDI)Mg(H₃BPPh₂)]₂; ¹⁵ (c) Synthesis of (H₃BPR¹R²BH₃)₂M(THF)₄ Complexes with R¹ = Ph; R² = CH(SiMe₃)₂; and M = Mg, Ca, and Sr¹⁷

dioxane)_{1.5} and K(H₃BP^tBu₂), where H₃BP^tBu₂BH₃⁻ is presumably formed via borane transfer from another unit of H₃BP^tBu₂⁻. Shortly after the report by Morris et al., Izod et al. reported how (H₃BPR¹R²BH₃)₂M(THF)₄ complexes with R¹ = Ph; R² = CH(SiMe₃)₂; and M = Mg, Ca, and Sr could be prepared in a similar stepwise route by treating dialkyl metal complexes like "Bu₂Mg with 2 equiv of R₁R₂PH·BH₃ followed by 2 equiv of BH₃·SMe₂ (Scheme 2c).¹⁷

As noted by us with trivalent uranium and lanthanides, ¹⁴ and by Izod et al. with alkaline earth metals, ¹⁷ metathesis reactions between metal iodides and lithium or potassium PDB salts do not proceed cleanly and are often low yielding in solvents such as Et₂O and THF. This likely accounts for why coordination complexes with phosphinodiboranate ligands have only emerged within the past decade. Recently, we reported how mechanochemical grinding ^{18,19} could be used to overcome these issues and form M-^tBu complexes in higher and more reproducible yields via salt metathesis reactions. ¹⁶ In addition to facilitating more routine access to pure ^tBu-PDB complexes, mechanochemical methods also allowed access to M-(H₃BPPh₂BH₃)₃ (M-Ph) complexes for the first time for comparative structural and spectroscopic analysis. ²⁰

Almost all the M-^tBu and M-Ph complexes reported to date form dimeric structures in the solid state, ^{16,20,21} which is unusual given the significant differences in ionic radii ranging from La³⁺ (1.032 Å) and U³⁺ (1.025 Å) to Lu³⁺ (0.861 Å).²² The only exceptions we have observed thus far are Ph-PDB complexes with U³⁺ and Ce³⁺; Ce-Ph is polymeric in the solid state, whereas both crystals of dimeric and polymeric U-Ph have been isolated.²⁰ Despite their solid-state similarities, more significant structural differences are observed for PDB

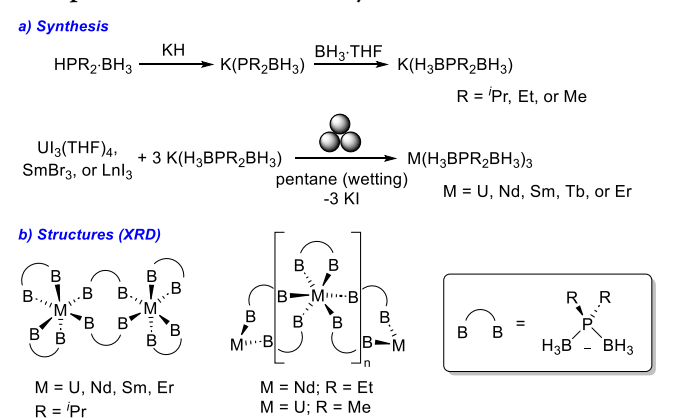
complexes in solution. ¹H and ¹¹B NMR studies have shown that dimeric PDB complexes break up into metal-dependent mixtures of monomers and dimers (or higher order oligomers) when dissolved in aromatic solvents. M-¹Bu complexes with the largest metal ions such as U³⁺, Ce³⁺, and Nd³⁺ appear to exist primarily as dimers in solution while smaller metal ions like Tb³⁺, Er³⁺, and Lu³⁺ exist primarily as monomers.²¹ M-Ph complexes with U³⁺ and the larger lanthanide ions Ce³⁺, Pr³⁺, and Nd³⁺ also appear to exist primarily as dimers when dissolved. However, it was not clear from these studies how the size of the substituents attached to phosphorus affects the degree of oligomerization in solution.

To more rigorously investigate the influence that phosphorus substituents have on the structure and reactivity of felement phosphinodiboranates, we expanded our initial investigation of M-tBu and M-Ph complexes reported previously to those reported here for the first time with smaller phosphorus substituents (M-iPr and M-Et). Our goal was to determine how a stepwise decrease in substituent size, especially from Bu to Pr to Et, affects the solid state and solution structures of f-element PDB complexes.²³ Here, we report the synthesis and characterization of ⁱPr-PDB complexes with U³⁺ (U-ⁱPr), Nd³⁺ (Nd-ⁱPr), Sm³⁺ (Sm-ⁱPr), Tb³⁺ (Tb-iPr), and Er3+ (Er-iPr) as well as Et-PDB complexes with U3+ (U-Et) and Nd3+ (Nd-Et). Our results show how steric and metal-size-induced variations in B-P-B angles, as quantified using single-crystal XRD and supporting density functional theory (DFT) calculations, appear to control the extent of oligomerization of trivalent f-element PDB complexes in solution.

RESULTS AND DISCUSSION

Synthesis and XRD Structures. The ligand starting materials $K(H_3BP^iPr_2BH_3)$ (^iPr-PDB) and $K(H_3BPEt_2BH_3)$ (Et-PDB) were synthesized by treating $HP^iPr_2 \cdot BH_3$ and $HPEt_2 \cdot BH_3$ with KH to form the phosphidoboranate, followed by the addition of $BH_3 \cdot THF$ (Scheme 3a). 6,7,24 The

Scheme 3. (a) General Synthesis of R-PDB Ligands and Metal Complexes and (b) Cartoon Showing the Arrangement of PDB Ligands and Degree of Solid-State Oligomerization Observed As a Function of Metal and Phosphorus Substituent Identity^a



^aWe note that B represents the relative location of the BH₃ groups and does not indicate anything about their denticity.

 $M(H_3BP^iPr_2BH_3)_3$ and $M(H_3BPEt_2BH_3)_3$ complexes (referred to as M- i Pr and M-Et, respectively, hereafter, where M=U or lanthanide) were prepared by ball milling 3 equiv of the corresponding potassium salt with $UI_3(THF)_4$, $SmBr_3$, or LnI_3 with several drops of pentane for wetting. 25 After grinding, the products were extracted and crystallized from Et_2O or CH_2Cl_2 , typically by vapor diffusion with pentane, in low to moderate yields (14–57%). As discussed below, the complexes adopt different structures in solution and the solid state (Scheme 3b), so we have used empirical formulas throughout when referencing the complexes for consistency.

Single-crystal XRD studies revealed that M- i Pr complexes with M = U, Nd, Sm, Tb, and Er crystallize in the monoclinic $P2_{1}/c$ space group and form isostructural dimers, as observed

previously for the $M(H_3BP^tBu_2BH_3)_3$ complexes (M^tBu) with $M = U^{3+}$ or Ln^{3+} . However, there are distinct structural differences due to the changes in alkyl substituent. For reference, M^tBu complexes maintain relatively symmetric bridging tBu -PDB ligands with similar M-B distances to both metals. They also alter the denticity of their chelating ligands from κ^2 -BH₃ to κ^1 -BH₃ to accommodate smaller metals.

In contrast to M-^tBu complexes, M-^tPr complexes adjust the denticity of their bridging ligands (not chelating) to accommodate different size metals, and the bridging ligands are asymmetric with one short M-B distance and one significantly longer M-B distance (Figure 1). The short M-B distances are consistent with those of κ^3 -BH₃, and they display a clear linear correlation when plotted against the metal radii (Figure 2a). In contrast, the longer M-B distances are consistent with κ^2 -BH₃ for ⁱPr-PDB complexes with smaller Er and Sm, but these shorten significantly for complexes with larger U and Nd consistent with a transition from κ^2 -BH₃ to κ^3 -BH₃ (Figure 2a). Averaging the four chelating M-B distances for each complex and plotting them against the ionic radius also reveals an excellent linear correlation ($R^2 = 0.998$; Figure 2a).²¹ Plots of the individual chelating M-B distances show how these distances adjust to accommodate a change in the size of the metal (Figure 2b).

As observed for the M-B distances, the size of the metal ion also has a significant influence on the bridging and chelating B-P-B angles. Bridging B-P-B angles in PDB complexes reported previously are larger than chelating B-P-B angles that bite down so the ligand can chelate to the metal. 16,20 The same is true for the ⁱPr-PDB and Et-PDB complexes reported here. The net difference in the larger bridging and smaller chelating B-P-B angles provides a parameter to quantify the inherent flexibility of the phosphinodiboranates and evaluate the influence of metal size on these angles. As shown in Figure 3, the difference between the bridging and average chelating B-P-B angles is the largest for the smallest metal in the series Er3+ (0.89 Å) at a difference of 16.5°, which emphasizes the remarkable flexibility of the Pr-PDB ligand. Plotting the difference in B-P-B angles against metal size reveals that the differences are highly correlated to metal size and decrease as the size of the metal ion increases from Er^{3+} (16.5°) to U^{3+} $(6.3^{\circ}).$

U(H₃BPEt₂BH₃)₃ (U-Et) and Nd(H₃BPEt₂BH₃)₃ (Nd-Et) were prepared as described for the ⁱPr-PDB complexes. Crystals of Nd-Et suitable for single-crystal XRD studies

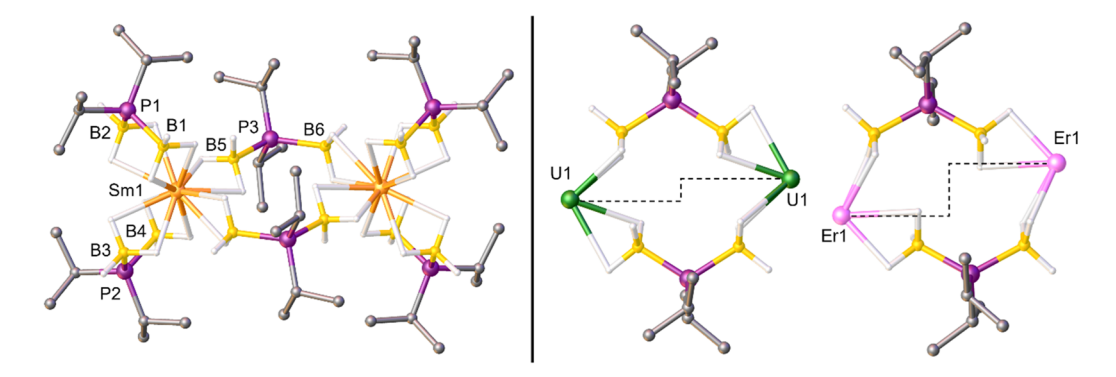


Figure 1. Left: Dimeric structure of $Sm(H_3BP^iPr_2BH_3)_3$ ($Sm^{-i}Pr$) from single-crystal XRD studies. Right: Comparison of bridging PDB ligands in the dimeric XRD structures of $U(H_3BP^iPr_2BH_3)_3$ ($U^{-i}Pr$) and $Er(H_3BP^iPr_2BH_3)_3$ ($Er^{-i}Pr$). The dashed line helps to emphasize the increasing asymmetry in the bridging iPr -PDB ligand with respect to metal binding. Hydrogen atoms attached to carbon were omitted. Ball and stick representation shown for easier viewing of all the atoms.

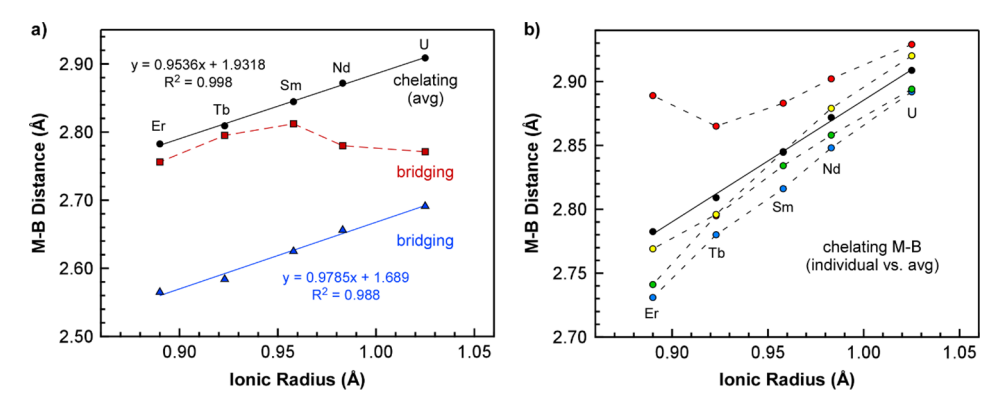


Figure 2. (a) Plot of chelating (average) and bridging M–B distances obtained from single-crystal XRD studies of $M(H_3BP^iPr_2BH_3)_3$ (M- iPr) complexes vs ionic radius of the corresponding metal (CN = 6). The distances associated with the bridging iPr -PDB ligands are denoted by red squares and blue triangles, and average distances associated with the chelating iPr -PDB ligands are represented by black circles. (b) Plot of all chelating M–B distances (colored circles) and average chelating M–B distances (black circles) vs ionic radius of the metal. Solid lines in both plots represent linear fits, whereas dashed lines are included to help guide the eye between data points.

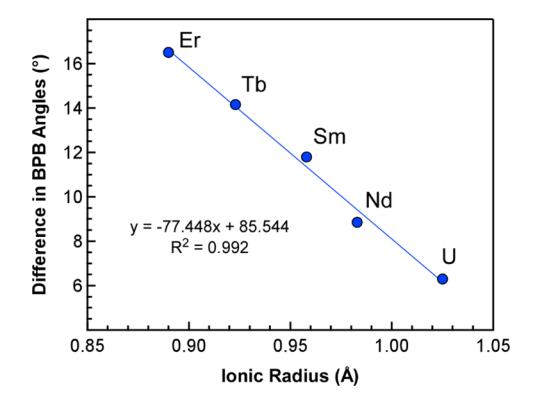


Figure 3. Difference in bridging and chelating B-P-B angles and in $M(H_3BP^iPr_2BH_3)_3$ ($M^{-i}Pr$) complexes plotted as a function of metal radii.

were isolated. Nd-Et has a polymeric structure that is markedly different compared to those of dimeric Nd-ⁱPr and Nd-^fBu (Figure 4). Each Nd³⁺ is coordinated by one chelating Et-PDB ligand and four bridging Et-PDB ligands. The chelating Nd–B distances are 2.933(6) Å, consistent with κ^2 -BH₃, whereas the two bridging Nd–B distances are different: the shorter distance suggests κ^3 -BH₃ (2.706(5) Å), whereas the longer

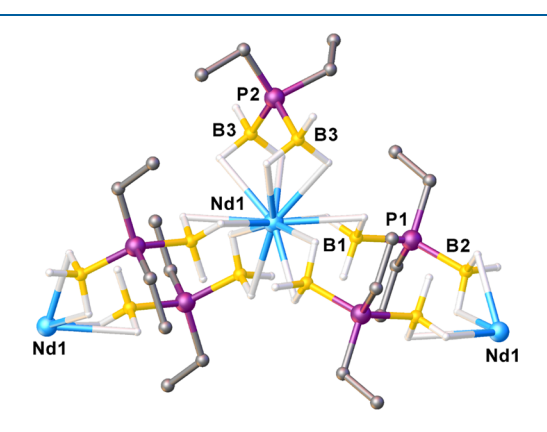


Figure 4. Polymeric structure of Nd(H₃BPEt₂BH₃)₃ (Nd-Et) from single-crystal XRD data. Hydrogen atoms attached to carbon and disordered components were omitted from the figure. Ball and stick representation shown for easier viewing of all the atoms.

distance suggests κ^2 -BH₃ (2.871(5) Å). As with dimeric structures such as Nd-ⁱPr, the bridging B-P-B angle at 120.6(3)° is larger than the chelating B-P-B angle at 109.2(4)°, giving a net difference of 11.4°.

Crystals of U-Et were not suitable for XRD studies, but we suspect that it adopts the same structure as Nd-Et based on IR comparison (see below) and separate crystallographic studies with U(H₃BPMe₂BH₃)₃ (U-Me). Prior to our discovery that ball milling reactions improve the yield of f-element PDB complexes, ¹⁶ we prepared U-Me in low yield by mixing UI₃(1,4-dioxane)_{1.5} with 3 equiv of K(H₃BPMe₂BH₃) in Et₂O (Figure S4, Supporting Information). XRD analysis of the few crystals that managed to be isolated revealed U-Me to be isostructural with Nd-Et (both crystallize in the C2/c space group). As with Nd-Et, the bridging U-B distances are asymmetric at 2.709(10) and 2.896(9) Å and the chelating U-B distances are 2.918(8) Å, consistent with κ^2 -BH₃ groups. The chelating and bridging B-P-B angles are 106.2(4)° and 118.6(4)°, respectively, to give a difference of 12.4°.

To better understand the influence of the phosphorus substituents on the structures of PDB complexes, we compared the bridging and chelating B–P–B angles of Nd-Et to those of Nd-ⁱPr described above and Nd-^tBu and Nd-Ph reported previously ^{16,20} by plotting them against the A value of each substituent (Figure 5). A values are experimentally derived

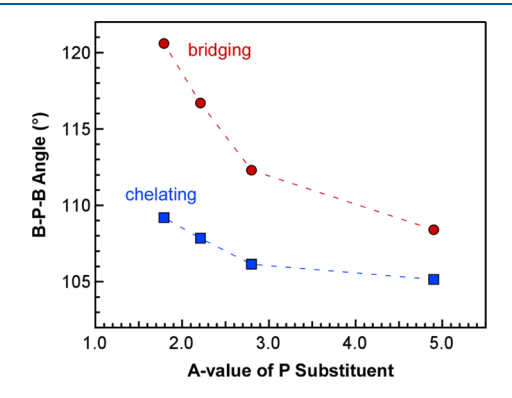


Figure 5. Plot of average bridging and chelating B–P–B angles of $Nd(H_3BPR_2BH_3)_3$ (R = Et, iPr , Ph, or iBu) obtained from single-crystal XRD studies vs the A values of the phosphorus substituents in kcal/mol. 26

Gibbs free energies (in kcal·mol⁻¹) associated with the axial/equatorial preference of cyclohexanes with differently sized substituents, ²⁶ and these values have long been used as a quantitative measure of steric bulk. A values decrease across the series in order of ¹Bu (4.9) > Ph (2.8) > ¹Pr (2.21) > Et (1.79). ²⁶ Consistently, both the bridging and chelating B-P-B angles are highly correlated to the A value of the phosphorus substituent and show a smooth decrease as the bulk increases from ethyl to *tert*-butyl. A similar trend is observed for the B-P-B angles in U complexes U-¹Bu, U-Ph, and U-¹Pr. These correlations indicate that increasing size and steric pressure of the phosphorus substituents decreases the flexibility of B-P-B angles in phosphinodiboranate ligands.

Spectroscopic Analysis. Infrared spectra collected on the new PDB complexes revealed the presence of terminal B–H and bridging B–H–M vibrational stretches between 2200 and 2500 cm⁻¹ (Figure 6), as is typically observed for borohydride

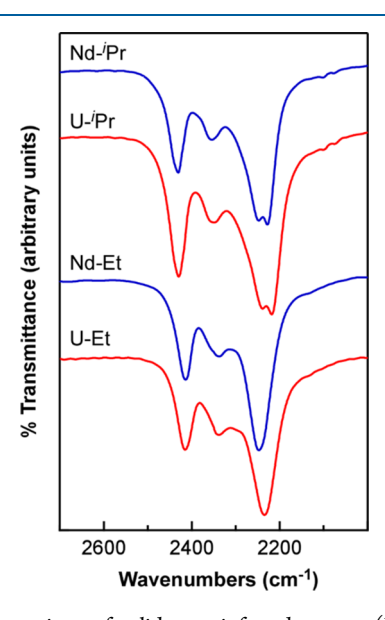


Figure 6. Comparison of solid-state infrared spectra (KBr) of U-ⁱPr and U-Et (red) and Nd-ⁱPr and Nd-Et (blue).

complexes.^{27,28} The spectrum of U-ⁱPr revealed four prominent B–H stretches at 2430, 2351, 2240, and 2218 cm⁻¹. Nd-ⁱPr revealed an identical spectral profile with stretching absorptions at 2432, 2354, 2248, and 2228 cm⁻¹. In contrast, the spectrum of U-Et revealed only three absorptions at 2414, 2339, and 2234 cm⁻¹, but the profile again matched the spectrum of the corresponding Nd complex (2414, 2339, and

2248 cm⁻¹) suggesting that U-Et and Nd-Et adopt similar solid-state structures. The terminal B—H stretches for each set of U and Nd complexes were identical within error, but the bridging B—H—M stretches for the U complexes were shifted to lower energy by 8–14 cm⁻¹. This could be attributed to a slight increase in M—H—B covalency for M = U vs M = Nd, but these data do not allow us to rule out other potential explanations such as metal-size-dependent changes in structure and Lewis acidity. In this context, we note that the two B—H—M stretching absorptions observed for U-ⁱPr and Nd-ⁱPr merge to form a single feature as the series is traversed in the order Sm-ⁱPr, Tb-ⁱPr, and Er-ⁱPr (Figure S27, Supporting Information).

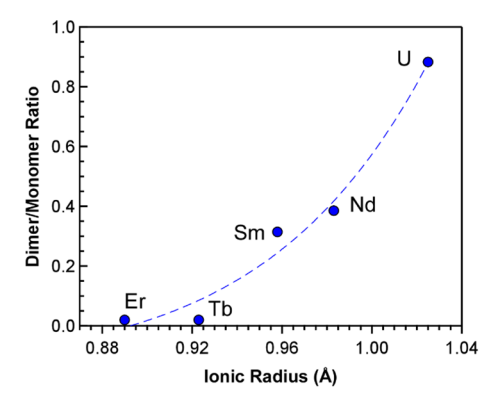
¹H and ¹¹B NMR data were collected on the M-ⁱPr and M-Et complexes to evaluate the effect of the phosphorus substituents on solution speciation and the degree of oligomerization. All five M-ⁱPr complexes revealed paramagnetically shifted ¹H and ¹¹B NMR resonances consistent with the presence of both a dimer and monomer in solution (Table 1). As with M-ⁱBu complexes, U-ⁱPr and Nd-ⁱPr with the largest metals showed the greatest ratio of dimer to monomer, whereas Tb-ⁱPr and Er-ⁱPr with the smallest metals in the series exist predominately as monomers. ¹H and ¹¹B NMR spectra collected on U-Et and Nd-Et again suggest both dimers and monomers, but the spectra indicate that the monomeric structures dominate in solution, contrasting observations made for U and Nd phosphinodiboranate complexes with larger phosphorus substituents.

Previous variable-temperature NMR studies of M-^tBu complexes in C₆D₆ revealed measurable differences in the dimer/monomer equilibrium for U^{3+} as compared with similarly sized lanthanide ions like La^{3+} and Ce^{3+} . Thermodynamic values obtained from Van't Hoff plots revealed ~1 kcal/ mol increase in the ΔH and ΔG for M = U, which was attributed to increased covalency in the U-H-B bonds.²¹ Unfortunately, NMR data collected on U-iPr and Nd-iPr revealed that iPr-PDB complexes are not as amenable to teasing out such small differences in the thermodynamic values (though DFT calculations were used to quantify these values; see below). NMR spectra for U-iPr and Nd-iPr showed additional resonances in the baseline that were not observed in the spectra of the ^tBu-PDB complexes. These resonances were concentration dependent and appeared most prominently in saturated solutions, and we suspect that they are likely attributed to higher order oligomers (e.g., trimer, tetramer). This hypothesis is consistent with the increased flexibility in the B-P-B angle for the Pr-PDB ligand that allow a wider

Table 1. ¹H and ¹¹B NMR Resonances for the BH₃ Groups in Each Complex in C₆D₆

	dimer		monomer		
complex	¹ H	¹¹ B	¹ H	¹¹ B	dimer/monomer molar ratio ^a
U- ⁱ Pr	74.2, 91.8	128.2, 298.1	95.1	186.6	0.88
Nd- ⁱ Pr	76.3, 77.1	69.9, 165.2	82.1	91.2	0.39
Sm- ⁱ Pr	-2.61, -1.74	-31.0^{b}	-3.67	-33.9	0.31
Tb- ⁱ Pr	not observed	-741.6, -502.2	-356.9	-546.5	0.02 ^c
Er- ⁱ Pr	not observed	-427.7, -234.3	-182.0	-270.5	0.02 ^c
U-Et	72.9, 86.6	140.1 ^b	89.5	192.5	0.04
Nd-Et	75.1, 76.9	73.5, 151.2	81.0	90.0	0.03

[&]quot;Based on ¹H NMR integrations measured of the BH₃ resonances at 20 °C unless stated otherwise. ^bSecond resonance unresolved or too weak to observe. ^cBased on ¹¹B NMR integrations at 20 °C.



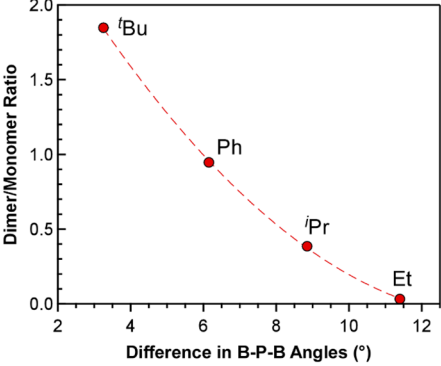


Figure 7. Left: Comparison of dimer/monomer ratios observed in the 1H NMR spectra of $M(H_3BP^iPr_2BH_3)_3$ ($M^{-i}Pr$) complexes in C_6D_6 plotted as a function of ionic radii of the metal (M=U, Nd, Sm, Tb, and Er; CN=6). Right: Comparison of dimer/monomer ratios observed in the 1H NMR spectra of $Nd(H_3BPR_2BH_3)_3$ complexes in C_6D_6 ($R=^tBu$, Ph, iPr , Et) plotted as a function of the difference in bridging and average chelating B-P-B angle.

range of structures to be adopted when compared to those with ${}^t\!\mathrm{Bu}\text{-PDB}.$

Though exact quantitative concentrations were not obtained from the NMR solutions, as needed for calculating equilibrium constants, we found it informative to conduct a coarse grain comparison of the dimer/monomer ratios to determine how the ratios change in response to PDB substituents and metal size. This analysis is possible because the PDB complexes have similar solubility in C₆D₆ (<5 mg/mL), and the dimers and monomers appear to be the major species present in solution. It is worth noting here that the two-to-one ratio of chelatingto-bridging PDB ligand resonances assigned as dimers could also be consistent with higher order oligomers that give the same ratio, similar to that reported by Mirkin and co-workers for dinuclear and tetranuclear Rh complexes.²⁹ We have so far been unable to rule out the possibility of these higher order oligomers for some of the phosphinodiboranate complexes (preliminary DOSY experiments were unsuccessful), but they appear unlikely, given that the dimers are isolated almost exclusively in the solid state. Moreover, our calculations described previously and below consistently suggest that dimers should be the dominant oligomer in solution. The only potential exception observed thus far is the Et-PDB complexes, as discussed in the following section (vide infra). However, given that these complexes appear to exist almost exclusively as monomers in solution on the NMR time scale, the identity of the oligomer should have little bearing on the analysis that follows.

We first compared the molar dimer/monomer ratio of the five i Pr-PDB complexes to their respective metal radii (Figure 7). As expected, the plot revealed a relatively smooth increase as the size of the trivalent metal radii increased from Er^{3+} to U^{3+} .

Next, we compared data for the neodymium complexes with Et-PDB and $^i\text{Pr-PDB}$ to those reported previously with $^i\text{Bu-PDB}$ and Ph-PDB to determine the influence of the substituents attached to phosphorus. The solid-state structures of all four Nd(H₃BPR₂BH₃)₃ complexes are known, 16,20 which allowed their dimer/monomer molar ratios obtained from NMR spectroscopy to be plotted against the difference in the chelating and bridging B–P–B angles from single-crystal XRD (Figure 7). The plot shows that the dimer/monomer ratio in solution is highly correlated to the substituent-dependent differences in B–P–B angles observed in the solid state.

Collectively, the plots in Figure 7 suggested that the degree of solution oligomerization, as measured by NMR spectroscopy, can be modeled using the difference in the bridging and average chelating B–P–B angle, a parameter that takes into account both the size of the metal and the size of the phosphorus substituent. Plotting all of the available data reported here and published previously supports this hypothesis (Figure 8). 16,20 The data can be fit to a power

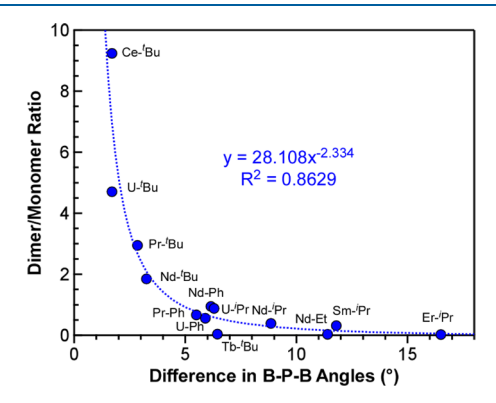


Figure 8. Comparison of dimer/monomer ratios observed in the 1H NMR spectra of all crystallographically characterized M- $(H_3BPR_2BH_3)_3$ complexes in C_6D_6 plotted as a function of the absolute difference in bridging and average chelating B-P-B angles.

law showing how the ratio of dimer to monomer increases and approaches infinity as the difference in the B-P-B angles goes to zero. These results suggest that the rigidity of the B-P-B angle, which can be tuned via the size and steric pressure of the phosphorus substituents, controls the extent of dimerization in solution with different trivalent f-metals.

Density Functional Theory (DFT) Calculations. DFT calculations were performed to further evaluate the structures of lanthanide and uranium PDB complexes and their comparative energies. Calculations allowed structures with differing degrees of oligomerization to be determined (including those not isolable experimentally) for comparison to the experimental results. Gas phase geometry optimization and harmonic vibrational analysis were performed using the TPSS-D3 functional and a basis set of near triple- ζ quality (see Experimental Section for details). When a solid-state structure was available, the geometry optimization was started from the coordinates obtained from the experiment.

The first series of calculations focused on the impact of the ligand and metal on the molecular geometry of the dimer. Though Nd-Et is a polymeric structure in the solid state, this complex was initially modeled as a dimer so that structural comparisons could be made with other dimeric Nd complexes with different substituents attached to phosphorus (Figure S28, Supporting Information). A similar choice was made for U-Et where no solid-state structure was obtained. Following the initial DFT optimizations from the solid-state structures, an extensive conformational search was performed using a computationally efficient method (specifically the GFN2-xTB tight binding approach) using the CREST algorithm³⁰ for the Nd-Et, Nd-Pr, Nd-Ph, and Nd-Bu dimers. The search resulted in 245, 114, 86, and 138 conformers within 6 kcal/mol at the GFN2-xTB level. The lowest energy conformer predicted by this lower level of theory was subsequently reoptimized with DFT (TPSS-D3). No conformational search could be performed with xTB methods for the U species since DFTB parameters are not available. Calculations involving U were computed by starting from the DFT optimized geometries obtained with Nd. Analogous conformational searches were performed for the other dimers studied (Er-iPr, Tb-iPr, and $Sm^{-i}Pr$).

Calculated structures for the ⁱPr-PDB dimers reproduced the most prominent structural features in the experimental data. All of the ⁱPr-PDB complexes showed the observed binding asymmetry in the bridging PDB ligands with one short M–B distance assigned as κ^3 -BH₃ and one long M–B distance assigned as κ^2 -BH₃. The chelating M–B distances also revealed a linear increase as the ionic radius of the metal increased (Figure 9, Table 2). The only significant distinction between

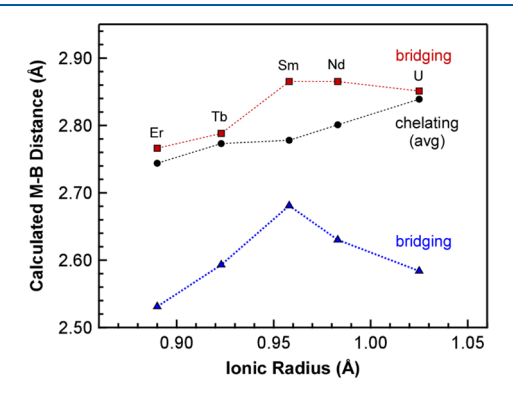


Figure 9. Plot of the DFT (TPSS-D3) calculated M–B distances in $M(H_3BP^iPr_2BH_3)_3$ vs the ionic radius of the corresponding metal (M = U, Nd, Sm, Tb, Er; CN = 6.).

the experimental and calculated structures is that one set of bridging M–B distances in the calculated structures are slightly longer than the chelating M–B distances (but still within the range for κ^2 -BH₃). Subtle differences in the linearity of the plotted data are also observed when comparing experimental and calculated plots of the shorter bridging M–B distances vs ionic radii. Collectively, these differences likely reflect small energy differences between various structural conformers. They could also indicate experimental solid-state packing effects not captured in the calculated data, as shown for other complexes with chelating borohydrides. The difference between chelating and bridging B–P–B angles was correlated with the ionic radii of the metals for the 'Pr-PDB complexes consistent with experimental results (Figure 3). The difference

Table 2. Selected Bond Distances (Å) and Ligand B-P-B Angles (deg) from the DFT (TPSS-D3) Optimized Structures of the Dimers

complex	M-B (Å) chelating	M-E brid		chelating angle	bridging angle	Δ angle
U- ^t Bu	2.846	2.599	2.754	104.9	113.6	8.7
U-Ph	2.807	2.574	2.837	109.9	118.1	8.2
U- ⁱ Pr	2.839	2.584	2.851	106.4	117.8	11.4
U-Et	2.787	2.685	2.900	110.9	118.6	7.6
Nd- ^t Bu	2.820	2.607	2.800	107.1	117.4	10.3
Nd-Ph	2.796	2.600	2.826	111.0	117.7	6.8
Nd- ⁱ Pr	2.801	2.630	2.865	110.1	118.7	8.6
Nd-Et	2.793	2.672	2.874	110.7	119.2	8.5
Sm- ⁱ Pr	2.778	2.681	2.865	110.5	116.9	6.4
Tb- ⁱ Pr	2.773	2.593	2.788	108.3	121.5	13.1
Er- ⁱ Pr	2.744	2.531	2.766	103.5	118.1	14.6

was higher for Er- i Pr (14.6°) and decreased to 8.6° for Nd- i Pr. For U- i Pr, the difference was slightly higher (11.4°) than that for Nd- i Pr.

We next compared the influence of R substituents on the structures of the calculated dimers. The average chelating U-B bond distances decreased in the order 'Bu > 'Pr > Ph > Et; the longest average chelating distance of 2.846 Å for U-^tBu decreased to 2.787 Å for U-Et to give a net difference of 0.059 Å across the series. The Nd complexes showed the same trend, decreasing in the order 'Bu > 'Pr > Ph > Et, but the net difference between largest and smallest average chelating Nd-B distances was smaller than for U ($\Delta = 0.027$ vs 0.059 Å). By comparison, the bridging Nd-B and U-B distances showed more variation and the relative ordering depended on the bridging bond distance in question. For example, the shorter bridging Nd-B distances decreased from 2.672 Å in Nd-Et to 2.600 Å in Nd-Ph, whereas the longer bridging Nd-B distances decreased from 2.874 Å in Nd-Et to 2.800 Å in Nd-^tBu. Similar ordering was observed for the bridging U–B distances, although with greater variation in the bond distances $(\Delta = 0.111 \text{ and } 0.146 \text{ Å})$ when compared to those in the Nd complexes ($\Delta = 0.072$ and 0.074 Å).

As observed in comparisons of the calculated Pr-PDB structures with different metals, the bridging and chelating B-P-B angles showed the same substituent-dependent trends as the experimental results, as exemplified with the A value plots for the Nd complexes in Figure 10. The magnitude of the calculated B-P-B angle differences, however, was generally smaller and had a few outliers. We note that the calculated angles represent those in the lowest energy structure obtained from the conformational search, and these could certainly be different in the solid state and solution, given the relatively small energy differences between multiple low energy conformers. In this context, we note that crystal packing and the associated intermolecular interactions are not included in the gas phase DFT calculations. Despite these differences, the gas phase calculations reproduce the general experimental trends and corroborate how B-P-B angles in PDB complexes are quite sensitive to the metal identity and phosphorus substituent size.

Although experimentally obtained thermodynamic data were not collected (*vide supra*), Gibbs free energies, enthalpies, and entropies of reaction were calculated using DFT (TPSS-D3) for $M_2(H_3BPR_2BH_3)_6 \rightarrow 2~M(H_3BPR_2BH_3)_3$ (R = Et, ⁱPr, Ph and ⁱBu; Table S7, Supporting Information). Solvent effects

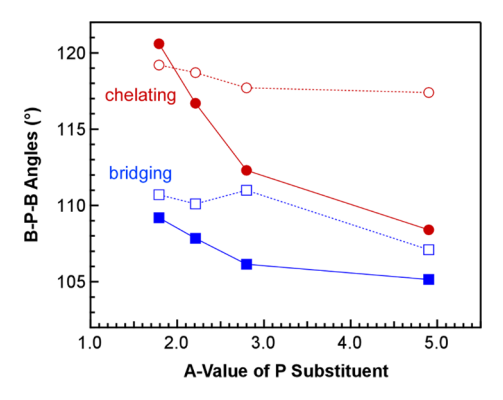


Figure 10. Comparison of B–P–B angles for Nd(H₃BPR₂BH₃)₃ plotted against the *A* values of the phosphorus substituents (given in kcal/mol). Experimental B–P–B angles are shown as solid lines and markers, and calculated angles are shown as dotted lines and open markers.

were included by performing a single point calculation with the COSMO model³² for benzene on the gas phase structure. For the [†]Pr-PDB complexes, the Gibbs free energy of the reaction tended to increase from the smallest metals Tb and Er to U, indicating that the dimer is more favorable for the larger ionic radii metals, consistent with the experiment. In contrast, Gibbs free energy and enthalpy calculations with different R groups and the same metal (Nd or U) were less consistent with the experimental dimer/monomer ratios observed by NMR spectroscopy (Table 3). U-Et and Nd-Et had the lowest

Table 3. Thermochemical Data at 298.15 K for the TPSS-D3 Free Energies, Enthalpies, and Entropies for Reaction Dimer \rightarrow 2 Monomer^a

complex	ΔG (kcal·mol ⁻¹)	$\Delta H \text{ (kcal·mol}^{-1}\text{)}$	$\Delta S \text{ (kcal·mol}^{-1} \cdot \text{K}^{-1}\text{)}$
U-Ph	9.2	24.8	0.059
Nd-Ph	8.7	24.1	0.058
$U^{-i}Pr$	8.7	23.6	0.057
U- ^t Bu	7.1	22.0	0.057
Nd- ^t Bu	6.6	20.7	0.054
U-Et	3.8	18.5	0.056
Nd- ⁱ Pr	3.6	18.1	0.055
Sm- ⁱ Pr	3.5	18.3	0.056
Nd-Et	1.8	16.0	0.054
Er- ⁱ Pr	1.0	15.7	0.056
Tb- ⁱ Pr	-0.2	14.6	0.056

^aFree energies have been computed by assuming a concentration of 1 M for all species taking benzene as the solvent.

calculated ΔG and ΔH values, in alignment with the greater experimental preference for monomers, but the values for U-Ph and Nd-Ph were calculated to be several kilocalories per mole larger than those for U-PBu and Nd-PBu with bulkier tertbutyl substituents. Moreover, the calculated values for U-PBu are also slightly higher than those for U-PBu, whereas Nd-PBu and Nd-PBu follow the experimental trend. These small discrepancies are likely attributed to different rotational conformations of the phenyl and isopropyl substituents, which are less isotropic compared to tert-butyl substituents. This is relevant given that the experimental dimer/monomer ratios represent a weighted average of deoligomerization energies for all of the conformational isomers present in

solution, whereas the calculations in Table 3 only capture energies associated with a single set of isomers.

Following the DFT study of the dimers, further computations were performed on Nd-Et. Recall that the experimental structure of Nd-Et is polymeric, with one of the PDB ligands in the typical dimer motif bridging to adjacent metals. NMR data suggested that Nd-Et dissolves to form the usual mixture of monomers and dimers, as observed for other PDB complexes, but the possibility that the bridging BH₃ group observed in the polymer remains unbound in solution to form a dimer with a "dangling" BH3 group was also considered. These "dangling" groups have been seen in the solid-state structure of other PDB complexes, 16,17,21 but only in the presence of competing donor ligands like THF. Indeed, as described in our previous reports, similar attempts to crystallize Nd-Et in the presence of THF resulted in adventitious crystals of Nd(H₃BPEt₂BH₃)₃(THF)₃ with dangling BH₃ groups (Figure S5, Supporting Information). Species with dangling BH₃ groups are also possible as part of the deoligomerization process and may be found along the reaction coordinate diagram. To evaluate the energy of these putative species, we performed calculations on the Nd-Et dimer with and without dangling BH₃ groups to compare their energies (isomers A and B, respectively, in Figure 11). The calculation revealed that isomer B is the energetically more stable isomer; isomer A has a higher free energy of 24.9 kcal/mol. This supports the hypothesis that deoligomerization of the solid-state polymer occurs when Nd-Et is dissolved to form mixtures of monomers and dimers (or higher order oligomers) with all BH₃ groups bound. Calculations on U-Et yielded similar results, with isomer B being favored by 22.7 kcal/mol in Gibbs's energy. These results suggest that species containing dangling BH3 groups are unlikely to persist in homoleptic PDB complexes containing these metals.

To further evaluate the structure in the solid state, computations were performed with a tetrameric oligomer (Nd-Et-4) as a model system of the solid (Scheme 4). Starting geometries were taken from the experimental polymeric Nd-Et structure (Figure S2). Note that a smaller basis set (def2-SVP) was used on light atoms due to the size of the tetramer. Given the prior results on the dimer, the ligands at the capping ends of the tetramer were truncated with chelating ligands since this is expected to be more favorable than leaving residual dangling bonds. A hypothetical oligomer, Nd-Pr-4, was also built by replacing Et-PDB ligands by Pr-PDB ligands. This structure was optimized with DFT to determine how the Nd-B distances and B-P-B angles change as a function of ligand choice in the larger model. Despite the differences between the polymeric experimental structure for Nd-Et and the calculated tetrameric structure of Nd-Et-4, the calculated and experimental bond distances and angles associated with the chelating and bridging Et-PDB bond distances are in relatively good agreement (see Supporting Information).

Calculations for the formation of the tetramers Nd-Et-4 and Nd-ⁱPr-4 from their corresponding dimers appear to account for the difference in solid-state structures of Nd-Et and Nd-ⁱPr (Scheme 4). In the case of Nd-Et, the free energy of the reaction is exergonic at -10.7 kcal/mol (an electronic energy difference of -33.1 kcal/mol), supporting that the formation of a tetramer is favorable for this system. While vibrational frequencies were not computed for Nd-ⁱPr-4 due to system size, the formation of this tetramer is uphill by +13.8 kcal/mol in electronic energy. Overall, these results are fully consistent

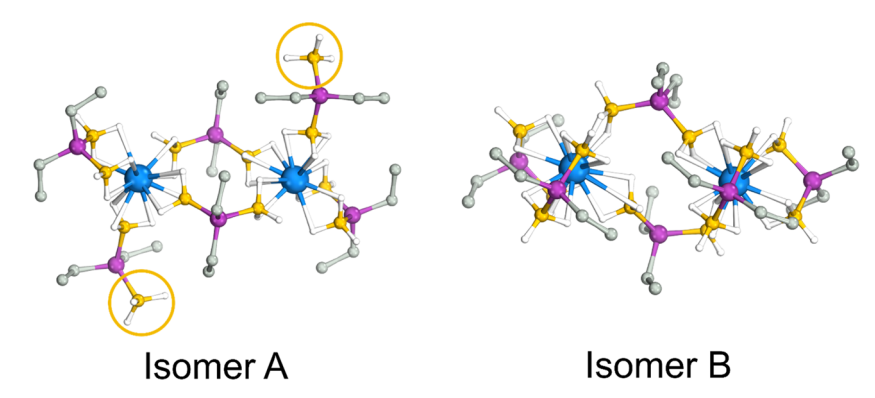


Figure 11. DFT optimized dimers of Nd-Et with different ligand coordination modes for Et-PDB. The orange circles highlight the dangling BH₃ groups. Hydrogen atoms attached to carbon have been omitted for clarity.

ı

Scheme 4. General Structures and Calculated Energies Associated with the Formation of Nd-Et-4 and Nd-ⁱPr-4 from Their Corresponding Dimers^a

 $^a\Delta E$ is shown instead of ΔG because the vibrational frequencies were not calculated for Nd-'Pr-4 due to the relatively large system size.

with experimental observations that Nd-Et exists as an extended coordination polymer in the solid state, whereas Nd-ⁱPr exists as a dimer. Moreover, they confirm how relatively subtle changes in the steric properties of phosphorus substituents can have a remarkable influence on the structure of phosphinodiboranate complexes.

CONCLUSIONS

In summary, we described the synthesis, structures, and solution speciation of homoleptic lanthanide and uranium phosphinodiboranates with isopropyl and ethyl substituents. Single-crystal XRD studies of the M(H₃BPⁱPr₂BH₃)₃ complexes with M = U, Nd, Sm, Tb, and Er revealed that they crystallize as dimers, whereas Nd(H3BPEt2BH3)3 and U-(H₃BPMe₂BH₃)₃ with smaller alkyl substituents crystallize as coordination polymers. Comparisons to M(H₃BP^tBu₂BH₃)₃ and M(H₃BPPh₂BH₃)₃ complexes reported previously show how the sizes of the metal and phosphorus substituents have a significant influence on the solution and solid-state structures. The stepwise decrease in steric bulk from $R = {}^{t}Bu$ to R = Etyields increased flexibility in the phosphinodiboranate B-P-B angles, as is evident by measured differences in chelating and bridging B-P-B angles when the identity of the metal is held constant. Moreover, decreasing the size of the metal in Pr-PDB complexes causes larger differences in chelating B-P-B angles that correlate to a decreasing ratio of dimer to monomer when the complexes are dissolved in benzene. The combined influence of both the phosphorus substituent size and metal radius on the preferred solution speciation of all known M(H₃BPR₂BH₃)₃ complexes can be modeled effectively using the difference in bridging and chelating B-P-B angles in the experimental structures. DFT calculations reproduce the

general experimental trends and showed that there is a relatively flat energy surface between many different conformers that likely contribute to experimentally observed differences in solution speciation. Free energy calculations comparing tetrameric and dimeric species account for the preferred adoption of polymeric and dimeric structures observed experimentally for Nd-Et and Nd-Pr.

Overall, these results demonstrate how steric changes to phosphorus substituents relatively far removed from metal coordination sites can have a significant influence on solution speciation, deoligomerization energies, and the solid-state structure of PDB complexes with trivalent f-metals. Though none of the phosphinodiboranate complexes reported here are appreciably volatile, these insights are important given that depolymerization energies are known to play a governing influence on the volatility in other f-element borohydride complexes,³³ including those containing aminodiboranates (the nitrogen congeners of phosphinodiboranates). 31,34-38 Moreover, the results may also have important implications for disubstituted diorganophosphinates (X₂PR₂⁻) containing metal-donor groups other than $X = BH_3$ (e.g., CR_2 , NR, O, S, and Se), especially those that have proven to be effective for trivalent f-element separations like dithiophosphinates (X = S).³⁹ Steric-induced changes in the solution speciation of phosphinate complexes would be expected to influence their solvent extraction properties. In this context, the underlying origin of how different phosphorus substituents influence the selectivity of dithiophosphinate extractants (including those with differently sized alkyl substituents) continues to be a subject of debate.39

■ EXPERIMENTAL SECTION

General Considerations. All reactions were carried out under an atmosphere of N₂ or Ar using glovebox or standard Schlenk techniques. All glassware was heated at 150 °C for at least 2 h and allowed to cool under a vacuum before use. Solvents were dried and deoxygenated using a Pure Process Technologies Solvent Purification System and stored over 3 Å molecular sieves. Deuterated solvents were deoxygenated on the Schlenk line by three freeze–pump—thaw cycles and stored over 3 Å molecular sieves for at least 3 days before use. K(H₃BP'Pr₂BH₃), K(H₃BPEt₂BH₃), and K(H₃BPMe₂BH₃) were prepared as described previously for K(H₃BPPh₂BH₃) and K-(H₃BP'Bu₂BH₃). ^{6,7} UI₃(THF)₄ was prepared as described previously from UCl₄. ⁴⁰ Anhydrous LnI₃ salts were purchased in their highest purity from Alfa Aesar or Strem Chemicals and used as received.

¹H NMR data were collected on a Bruker AVANCE-400 operating at 400 MHz or a Bruker AVANCE-500 operating at 500 MHz. The ¹¹B NMR data were collected on a Bruker AVANCE-400 operating at

128 MHz or a Bruker AVANCE-500 operating at 160 MHz. Chemical shifts in C_6D_6 are reported in δ units relative to those in C_6D_5H (1H ; δ 7.16 ppm) and BF₃·Et₂O (¹¹B; δ 0.0 ppm). ³¹P NMR data were not collected because these resonances are typically too broad to be observed for paramagnetic phosphinodiboranate complexes due to paramagnetic broadening and coupling with the quadrupolar ¹⁰B and ¹¹B nuclei. Microanalytical data (CHN) were collected using an EAI CE-440 elemental analyzer at the University of Iowa's Shared Instrumentation Facility. IR spectra were acquired with a Thermo Scientific Nicolet iS5 in a N2-filled glovebox as KBr pellets. Mechanochemical reactions were carried out on a Form-Tech Scientific (FTS) FTS1000 shaker mill or a FlackTek SpeedMixer with a Teflon insert designed to accommodate FTS grinding jars. All mechanochemical reactions were conducted in 5 mL stainless steel "SmartSnap" (hermetic seal) grinding jars from FTS using two 5 mm stainless steel balls (304 grade) for grinding. Melting points were collected in sealed capillaries using a REACH melting point apparatus.

Tris(diisopropylphosphinodiboranato)neodymium(III), Nd- $(H_3BP'Pr_2BH_3)_3$ (Nd-'Pr). NdI_3 (0.100 g, 0.190 mmol) and $K(H_3BP^iPr_2BH_3)$ (0.105 g, 0.571 mmol) were loaded into a 5 mL FTS ball-milling jar with two 5 mm stainless steel balls and a few drops of pentane as a wetting solvent. The jars were hermetically sealed with electrical tape, transferred to a FlackTek SpeedMixer, and milled three times at 1800 rpm for 5 min each. The jar was transferred to a glovebox and opened to reveal a light blue paste. The crude mixture was suspended in Et₂O, filtered, and evaporated to dryness under a vacuum to afford a light blue oil. The product was dissolved in a minimum amount of Et_2O and stored in a freezer at -30 °C. Small, light blue blocks formed after 2 days. Yield: 62.4 mg (57%). Mp: 150 °C. Anal. calcd for C₁₈H₆₀B₆P₃Nd: C, 37.36; H, 10.45. Found: C, 36.95; H, 10.61. ¹H NMR (500 MHz, C_6D_6 , δ): 1.12 (br s, $CH(CH_3)_2$), 1.60 (br s, $CH(CH_3)_2$), 1.78 (br s, $CH(CH_3)_2$), 2.43 (br s, CH(CH₃)₂), 3.28 (br s, CH(CH₃)₂), 4.88 (br s, CH(CH₃)₂), 76.3 (br s, BH₃, dimer), 77.1 (br s, BH₃, dimer), 82.1 (br s, BH₃, monomer). ¹¹B NMR (160 MHz, C_6D_6 , δ): 69.9 (br s, BH₃, dimer), 91.2 (br s, BH₃, monomer), 165.2 (br s, BH₃, dimer). IR (KBr) $\overline{\nu}_{\rm max}$ (cm⁻¹): 2961 (s), 2931 (m), 2896 (w), 2871 (m), 2432 (vs), 2354 (s), 2248 (vs), 2228 (vs), 1462 (s), 1386 (m), 1382 (w), 1233 (s), 1159 (w), 1062 (s), 1036 (m), 929 (w), 884 (m), 799 (m), 727 (m), 679 (s).

Tris(diisopropylphosphinodiboranato)uranium(III), U-(H₃BPⁱPr₂BH₃)₃ (U-ⁱPr). Prepared as described for Nd-ⁱPr with UI₃(THF)₄ (0.100 g, 0.110 mmol) and K(H₃BPⁱPr₂BH₃) (0.061 g, 0.330 mmol). Yield: 17.3 mg (23%). M.p.: 150 °C (dec). Anal. calcd for $C_{18}H_{60}B_6P_3U$: C, 32.15; H, 8.99. Found: C, 32.43; H, 8.50. ¹H NMR (500 MHz, C_6D_6 , δ): 0.94 (br s, CH(CH₃)₂), 1.05 (br s, CH(CH₃)₂), 2.30 (br s, CH(CH₃)₂), 2.73 (br s, CH(CH₃)₂), 3.95 (br s, CH(CH₃)₂), 74.2 (br s, BH₃, dimer), 91.8 (br s, BH₃, dimer), 95.1 (br s, BH₃, monomer). ¹¹B NMR (160 MHz, C_6D_6 , δ): 128.2 (br s, dimer, chelating), 186.6 (br s, monomer), 298.1 (br s, dimer, bridging). IR (KBr) $\bar{\nu}_{max}$ (cm⁻¹): 2959 (s), 2932 (s), 2894 (s), 2871 (s), 2430 (vs), 2351 (s), 2240 (vs), 2218 (vs), 1462 (s), 1384 (m), 1367 (m), 1231 (s), 1183 (w), 1159 (w), 1131 (w), 1102 (w), 1060 (s), 1034 (s), 927 (w), 884 (m), 795 (m), 727 (s), 677 (s).

Tris(diethylphosphinodiboranato)uranium(III), U-(H₃BPEt₂BH₃)₃ (U-Et). Prepared as described for Nd-¹Pr with UI₃(THF)₄ (0.100 g, 0.110 mmol) and K(H₃BPEt₂BH₃) (0.052 g, 0.330 mmol). Yield: 14.8 mg (18%). ¹H NMR (500 MHz, C₆D₆, δ): 0.22 (br s, CH₂CH₃, monomer), 0.43 (br s, CH₂CH₃, monomer), 1.50 (br s, CH₂CH₃, dimer), 1.58 (br s, CH₂CH₃, dimer), 3.60 (br s, CH₂CH₃, dimer), 72.9 (br s, BH₃, dimer, chelating), 86.6 (br s, BH₃ dimer, bridging), 89.5 (br s, BH₃, monomer). ¹¹B NMR (160 MHz, C₆D₆, δ): 140.1 (br s, dimer); 192.5 (br s, monomer). IR (KBr) $\overline{\nu}_{\text{max}}$ (cm⁻¹): 2971 (s), 2938 (s), 2911 (m), 2880 (m), 2414 (vs), 2339 (s), 2234 (vs), 1455 (m), 1413 (w), 1379 (w), 1258 (m), 1219 (s), 1174 (s), 1128 (s), 1071 (s), 1037 (s), 1013 (s), 785 (s), 741 (w), 679 (s).

Tris(diethylphosphinodiboranato)neodymium(III), Nd-(H₃BPEt₂BH₃)₃ (Nd-Et). Prepared as described for Nd-Pr with NdI₃ (0.100 g, 0.110 mmol) and K(H₃BPEt₂BH₃) (0.061 g, 0.330 mmol). Yield: 17.3 mg (23%). Anal. calcd for C₁₂H₄₈B₆P₃Nd: C,

29.14; H, 9.78. Found: C, 28.70; H, 9.44. 1 H NMR (500 MHz, C_6D_6 , δ): 0.68 (br s, CH₂CH₃, dimer), 1.20 (br s, CH₂CH₃, monomer), 1.54 (br s, CH₂CH₃, dimer), 1.84 (br s, CH₂CH₃, dimer), 2.08 (br s, CH₂CH₃, monomer), 3.88 (br s, CH₂CH₃, dimer), 75.1 (br s, BH₃, dimer, bridging), 76.9 (br s, BH₃, dimer, chelating), 81.0 (br s, BH₃, monomer). 11 B NMR (160 MHz, C_6D_6 , δ): 73.5 (br s, dimer), 90.0 (br s, monomer), 151.2 (br s dimer). IR (KBr) $\bar{\nu}_{max}$ (cm⁻¹): 2972 (s), 2938 (s), 2911 (m), 2879 (m), 2414 (vs), 2339 (s), 2248 (vs), 1456 (s), 1412 (m), 1379 (m), 1260 (w), 1222 (s), 1177 (m), 1129 (m), 1071 (s), 1036 (s), 1033 (s), 786 (s), 737 (w), 676 (s).

Tris(diisopropylphosphinodiboranato)samarium(III), Sm-(H₃BPⁱPr₂BH₃)₃ (Sm-ⁱPr). Prepared as described for Er-ⁱPr using SmBr₃ (0.103 g, 0.264 mmol) and K(H₃BPⁱPr₂BH₃) (0.142 g, 0.772 mmol). Vapor diffusion with DCM and pentane at −30 °C yielded small clear blocks that were isolated after approximately 20 days. Yield: 52.2 mg (34%). ¹H NMR (400 MHz, C_6D_6 , δ): -3.67 (br q, BH₃, monomer), -2.61 (br d, BH₃, dimer, chelating), -1.74 (br q, BH₃, dimer, bridging), 1.00 (s, CH(CH₃)₂, dimer), 1.23 (s, CH(CH₃)₂, monomer), 1.66 (s, CH(CH₃)₂, dimer), 1.95 (s, CH(CH₃)₂, monomer). ¹¹B NMR (128 MHz, C_6D_6 , δ): -33.9 (br s, fwhm = 320 Hz, monomer), -31.0 (br s, dimer). IR (KBr) $\overline{\nu}_{max}$ (cm⁻¹): 2969 (vs), 2960 (vs), 2931 (s), 2813 (w), 2763 (w), 2732 (w), 2723 (w), 2431 (vs), 2398 (w), 2359 (s), 2247 (br), 2228 (vs), 1463 (s), 1386 (s), 1366 (m), 1292 (w), 1240 (vs), 1185 (m), 1159 (m), 1101 (w), 1078 (w), 1060 (vs), 1036 (m), 1026 (m), 966 (w), 928 (m), 885 (s), 797 (m), 771 (m), 727 (s), 711 (m), 680 (vs), 653 (m), 638 (m), 629 (w).

Tris(diisopropylphosphinodiboranato)terbium(III), Tb-(H₃BP'Pr₂BH₃)₃ (Tb-'Pr). TbI₃ (0.100 g, 0.185 mmol) and $K(H_3BP^iPr_2BH_3)$ (0.103 g, 0.560 mmol) were loaded into a 5 mL FTS ball-milling jar with two 5 mm stainless steel balls and approximately 15 drops of pentane. The jar was hermetically sealed using electrical tape, transferred to an FTS shaker mill, and milled for 90 min at 1800 rpm. The jar was transferred to a glovebox and opened to reveal a gray paste. The contents were suspended in Et₂O (15 mL), stirred for 15 min, and filtered through a plug of Celite. Pentane (20 mL) was added to the clear solution to precipitate the unreacted ligand salt, and the mixture was stirred for 45 min. The mixture was filtered, the filtrate was evaporated to dryness under a vacuum, and the residue was dissolved in DCM (5 mL). Vapor diffusion with pentane at -30 °C yielded small clear blocks after five months when the laboratory was reopened after the COVID-19 shutdown. Yield: 15.2 mg (14%). 1H NMR (400 MHz, C_6D_6 , δ): -356.9 (br s, fwhm = 7000 Hz, BH₃), -2.03 (br s, fwhm = 110 Hz, CH(CH₃)₂, monomer), 1.13 (br s, fwhm = 110 Hz, CH(CH₃)₂, monomer), 14.33 (br s, dimer), 15.18 (br s, dimer). 11B NMR (128 MHz, C_6D_6 , δ): -741.6 (br s, dimer, bridging), -546.5 (br s, fwhm = 520 Hz, monomer), and -502.2 (br s, dimer, chelating). IR (KBr) $\overline{\nu}_{\text{max}}$ (cm⁻¹): 2968 (vs), 2931 (s), 2896 (s), 2871 (s), 2813 (w), 2763 (w), 2732 (w), 2723 (sh), 2434 (s), 2404 (w), 2361 (m), 2341 (w), 2258 (sh), 2229 (vs), 1462 (vs), 1386 (m), 1365 (m), 1245 (vs), 1158 (m), 1143 (sh), 1102 (w), 1060 (vs), 1037 (m), 1025 (m), 966 (w), 927 (m), 885 (s), 798 (m), 772 (m), 728 (m), 704 (w), 683 (vs), 651 (w), 639 (m).

Tris(diisopropylphosphinodiboranato)erbium(III), Er-(H₃BPⁱPr₂BH₃)₃ (Er-iPr). ErI₃ (0.100 g, 0.182 mmol) and K-(H₃BPⁱPr₂BH₃) (0.103 g, 0.560 mmol) were loaded into a 5 mL FTS ball-milling jar with two 5 mm stainless steel balls and approximately 15 drops of pentane. The jar was hermetically sealed, transferred to a FlackTek SpeedMixer, and milled three times at 1800 rpm for 5 min for each cycle. The jar was transferred to a glovebox and opened to reveal a gray paste. The contents were suspended in Et₂O (15 mL), stirred for 15 min, and filtered through a plug of Celite. Pentane (20 mL) was added to the light pink solution with stirring, which yielded a precipitate presumed to be an unreacted ligand salt. The mixture was filtered through a plug of Celite, and the filtrate was evaporated to dryness under vacuum. The residue was dissolved in DCM (5 mL). Vapor diffusion with pentane at −30 °C yielded small pink blocks that were collected after one month. Yield: 41.1 mg (38%). ¹H NMR (400 MHz, C_6D_6 , δ): -182.0 (br s, fwhm =

9000 Hz, BH₃, monomer), -4.75 (br s, CH(CH₃)₂, dimer, bridging), 3.42 (br s, fwhm = 75 Hz, CH(CH₃)₂, monomer), 10.68 (br s, CH(CH₃)₂, dimer, chelating). ¹¹B NMR (128 MHz, C₆D₆, δ): -427.7 (br s, dimer, bridging), -270.5 (br s, fwhm = 320 Hz, monomer), -234.3 (br s, dimer, chelating). IR (KBr) $\overline{\nu}_{max}$ (cm⁻¹): 2967 (vs), 2961 (vs), 2931 (s), 2896 (m), 2872 (s), 2849 (w), 2812 (w), 2763 (w), 2733 (w), 2721 (w), 2438 (vs), 2420 (w), 2409 (s), 2368 (m), 2346 (w), 2251 (sh), 2232 (vs), 1463 (s), 1451 (sh), 1386 (m), 1365 (m), 1262 (m), 1247 (vs), 1159 (m), 1135 (w), 1102 (w), 1062 (vs), 1053 (sh), 1038 (s), 1026 (m), 967 (w), 928 (m), 885 (m), 800 (m), 729 (m), 705 (w), 686 (s), 649 (m), 642 (m).

Tris(dimethylphosphinodiboranato)uranium(III), U-(H₃BPMe₂BH₃)₃ (U-Me). UI₃(1,4-dioxane)_{1.5} (0.105 g, 0.140 mmol) and K(H₃BPMe₂BH₃) (0.0569 g, 0.452 mmol) were stirred in Et₂O overnight. The reaction mixture was evaporated to dryness under a vacuum and extracted with Et₂O. The mixture was filtered and layered with pentane to yield a few small, dark red prisms that were suitable for XRD analysis. This chemistry was investigated prior to our discovery that mechanochemical methods are more effective for preparing PDB complexes in higher yields for analysis. This reaction was not revisited for further optimization and more thorough characterization, but we wish to report the structure of U-Me here for comparison given its parallels to the structure of Nd-Et.

Crystallographic Studies. Single-crystal X-ray diffraction data were collected as previously described. 14,16,20,21 All crystallographic data except those for Tb-Pr were collected on a Bruker Nonius Kappa ApexII instrument equipped with a charge-coupled-device (CCD) detector. The data for Tb(H₃BPⁱPr₂BH₃)₃ were collected on a Bruker D8 Venture Duo instrument equipped with a Bruker photon III detector. Both instruments were equipped with graphite monochromatized Mo K α radiation ($\lambda = 0.71073$ Å). Samples of Nd-ⁱPr and U-Me were cooled to 180 and 190 K, respectively, using an Oxford Cryostream 700 low temperature device. All other samples were cooled to 150 K. Data were collected using phi and omega scans and corrected for absorption using redundant reflections and the SADABS⁴¹ program. Structures were solved with intrinsic phasing (SHELXT)⁴² and subsequent least-squares refinement (SHELXL),⁴³ which confirmed the positions of all non-hydrogen atoms. All hydrogen atom positions were idealized and allowed to ride on the attached carbon and boron atoms. B-H distances were fixed at 1.20 Å. Structure solution and refinement were performed with Olex2.44 Publication figures were made using Mercury version 4.3.1 or Olex2. 44,45 Crystallographic data and refinement details for each structure are provided in Table S1 in the Supporting Information.

Computational Details. Prior to DFT geometry optimizations, a low-level DFT-tight binding (GFN2-xTB) conformational search was performed for monomer and dimer structures of Nd-Et, Nd-iPr, Nd-Ph, and Nd-^tBu complexes using the Conformer-Rotamer Ensemble Sampling Tool (CREST) in the xtb program.³⁰ The lowest energy conformer for the monomer was taken as the starting structure for subsequent optimization with DFT. In the case of the dimers, starting geometries were taken both from available X-ray diffraction structures and from the lowest conformer predicted by CREST. For each dimer, the two structures were optimized, and that with the lowest energy was used in subsequent analysis. DFT geometry optimizations were performed, followed by harmonic vibrational analysis. All structures were confirmed as minima (with few exceptions, vide infra), and free energies are reported using the standard harmonic oscillator, rigid rotor approximations. The TPSS functional with Grimme's D3 correction was employed (TPSS-D3) with the original damping function. The resolution of identity (RI) approximation was used for integral evaluation. 46-50 The def2-TZVP basis is used on all atoms with the exception of uranium where the def-TZVP basis was used for uranium and for carbon where the def2-SV(P) basis was used. 51-The smaller basis set is used on carbon to reduce the computational cost for the largest dimers. For the model oligomers of Nd-Et and Nd-iPr, molecular geometries were optimized with def2-TZVP on Nd and def2-SV(P) for all other atoms using same functional. Once more, this was due to system size and the resulting computational cost. The SCF energy was converged to 10^{-7} a.u., and the Cartesian gradient

was converged to 10^{-4} a.u. Single point calculations including the conductor-like screening model (COSMO)³² were performed on the gas phase geometries to account for solvation using a dielectric constant of 2.274 for benzene. All DFT calculations were performed as implemented in the Turbomole program package. Some of the dimers have very small (<15 cm⁻¹) imaginary modes associated with methyl rotations. These do not impact the computed free energies since the quasiharmonic correction suggested by Cramer and Truhlar in which all normal modes less than 100 cm^{-1} are replaced with 100 cm^{-1} is employed.⁵⁹ Specifically, free energies were corrected using the single point energies in benzene, computed at 298.15 K, and assumed a concentration of 1 M for all reactants and products.

ASSOCIATED CONTENT

Data Availability Statement

A data set collection of computational results is available in the ioChem-BD repository⁶⁰ and can be accessed online using the following link (https://iochem-bd.bsc.es/browse/review-collection/100/305319/68e20fc7fd8dc58691e7d63f). The input and output files are also available in the FigShare repository (https://figshare.com/s/a98c4ccb7d38476600c0)

Solution Supporting Information

The Supporting Information is available free of charge at https://pubs.acs.org/doi/10.1021/acs.inorgchem.3c02773.

Optimized structures (ZIP)

Crystallographic details, NMR and IR spectra, tabulated DFT data and structures (PDF)

Accession Codes

CCDC 2283040-2283047 contain the supplementary crystallographic data for this paper. These data can be obtained free of charge via www.ccdc.cam.ac.uk/data_request/cif, or by emailing data_request@ccdc.cam.ac.uk, or by contacting The Cambridge Crystallographic Data Centre, 12 Union Road, Cambridge CB2 1EZ, UK; fax: +44 1223 336033.

AUTHOR INFORMATION

Corresponding Authors

Bess Vlaisavljevich — Department of Chemistry, The University of South Dakota, Vermillion, South Dakota 57069, United States; Orcid.org/0000-0001-6065-0732; Email: Bess.Vlaisavljevich@usd.edu

Scott R. Daly — Department of Chemistry, The University of Iowa, Iowa 52242, United States; orcid.org/0000-0001-6229-0822; Email: scott-daly@uiowa.edu

Authors

Joshua C. Zgrabik – Department of Chemistry, The University of Iowa, Iowa 52242, United States

Rina Bhowmick – Department of Chemistry, The University of South Dakota, Vermillion, South Dakota 57069, United States

Francesca D. Eckstrom – Department of Chemistry, The University of Iowa, Iowa 52242, United States

A. Rayford Harrison — Department of Chemistry, The University of Iowa, Iowa 52242, United States; orcid.org/0000-0001-8369-9002

Taylor V. Fetrow – Department of Chemistry, The University of Iowa, Iowa 52242, United States

Anastasia V. Blake — Department of Chemistry, The University of Iowa, Iowa 52242, United States

Complete contact information is available at: https://pubs.acs.org/10.1021/acs.inorgchem.3c02773

Notes

The authors declare no competing financial interest.

ACKNOWLEDGMENTS

This material is based upon work supported by the U.S. Department of Energy (DOE), Office of Science, Office of Basic Energy Sciences, Separation Science program under Award DE-SC0019426. We thank Dale Swenson for collecting the single-crystal XRD data. The structure of Tb(H₃BPⁱPr₂BH₃)₃ was collected using the instrument supported by NSF CHE-1828117. Some of the NMR data were collected using the instrument supported by NSF CHE-2017828. Calculations were performed using the High-Performance Computing systems at the University of South Dakota, which is funded by NSF Award OAC-1626516. Bess Vlaisavljevich and Rina Bhowmick acknowledge that the land their research was performed on is the original homelands of the Dakota, Lakota, and Nakota tribal nations.

REFERENCES

- (1) Thompson, N. R. The preparation and some reactions of potassium phosphinidodiborane and potassium dimethylphosphinidobis(trimethylboron). *J. Chem. Soc.* 1965, 6290–6295.
- (2) Gilje, J. W.; Morse, K. W.; Parry, R. W. Preparation and structure of ammonia and alkylamine addition compounds of phosphine diborane, B₂H₆.PH₃.NR₃. *Inorg. Chem.* **1967**, *6*, 1761–1765.
- (3) Fritz, G.; Pfannerer, F. Chemistry of boron-phosphorus compounds. Z. Anorg. Allg. Chem. 1970, 373, 30–35.
- (4) Mayer, E.; Laubengayer, A. W. Reaction of phosphine borane, phenylphosphine borane, and phosphonium iodide with sodium tetrahydridoborate. *Monatsh. Chem.* **1970**, *101*, 1138–1144.
- (5) Keller, P. C.; Schwartz, L. D. Preparation and properties of lithium bis(borane)dimethylphosphide(1-). *Inorg. Chem.* **1971**, *10*, 645–647.
- (6) Dornhaus, F.; Bolte, M. (18-Crown-6) potassium di-tert-butylphosphanylbisborohydride. *Acta Crystallogr., Sect. E: Struct. Rep. Online* **2006**, 62, m3573–m3575.
- (7) Dornhaus, F.; Bolte, M.; Lerner, H.-W.; Wagner, M. Phosphanylborohydrides: first assessment of the relative Lewis basicities of [BH₃PPh₂]⁻, CH₃PPh₂, and HPPh₂. *Eur. J. Inorg. Chem.* **2006**, 2006, 1777–1785.
- (8) Anstey, M. R.; Corbett, M. T.; Majzoub, E. H.; Cordaro, J. G. Improved synthesis of bis(borano)hypophosphite salts. *Inorg. Chem.* **2010**, *49*, 8197–8199.
- (9) Izod, K.; Watson, J. M.; El-Hamruni, S. M.; Harrington, R. W.; Waddell, P. G. Alkali-metal- and alkaline-earth-metal-mediated C-O activation of an anisole-substituted phosphido-borane ligand. *Organometallics* **2017**, *36*, 2218–2227.
- (10) Hofstoetter, H.; Mayer, E. Synthesis and structure of associated μ -phosphinodiborane and of derivatives substituted at the phosphorus. *Monatsh. Chem.* **1974**, *105*, 712–725.
- (11) Butenschon, H.; Kohser, S. C.; Gopal Dongol, K. Synthesis of spiro annelated isochromanones by ring expansion of benzocyclobutenones in the presence of lithium diisopropylphosphide. *Heterocycles* **2007**, *74*, 339–350.
- (12) Gamble, E. L.; Gilmont, P. Preparation and properties of diborane diphosphine. *J. Am. Chem. Soc.* **1940**, *62*, 717–721.
- (13) Maser, L.; Flosdorf, K.; Langer, R. Synthesis and reactivity of iron(II) hydride complexes containing diphenylphosphine ligands. *J. Organomet. Chem.* **2015**, 791, 6–12.
- (14) Blake, A. V.; Fetrow, T. V.; Theiler, Z. J.; Vlaisavljevich, B.; Daly, S. R. Homoleptic uranium and lanthanide phosphinodiboranates. *Chem. Commun.* **2018**, *54*, 5602–5605.
- (15) Morris, L. J.; Hill, M. S.; Mahon, M. F.; Manners, I.; Patrick, B. O. Alkaline-Earth Derivatives of Diphenylphosphine-Borane. *Organometallics* **2020**, *39*, 4195–4207.

- (16) Fetrow, T. V.; Bhowmick, R.; Achazi, A. J.; Blake, A. V.; Eckstrom, F. D.; Vlaisavljevich, B.; Daly, S. R. Chelating Borohydrides for Lanthanides and Actinides: Structures, Mechanochemistry, and Case Studies with Phosphinodiboranates. *Inorg. Chem.* **2020**, *59*, 48–61.
- (17) Izod, K.; Watson, J. M.; Harrington, R. W.; Clegg, W. Phosphido-bis(borane) complexes of the alkaline earth metals. *Dalton Trans.* **2021**, *50*, 1019–1024.
- (18) Rightmire, N. R.; Hanusa, T. P. Advances in organometallic synthesis with mechanochemical methods. *Dalton Transactions* **2016**, 45, 2352–2362.
- (19) Fiss, B. G.; Richard, A. J.; Douglas, G.; Kojic, M.; Friscic, T.; Moores, A. Mechanochemical methods for the transfer of electrons and exchange of ions: inorganic reactivity from nanoparticles to organometallics. *Chem. Soc. Rev.* **2021**, *50*, 8279–8318.
- (20) Fetrow, T. V.; Daly, S. R. Mechanochemical synthesis and structural analysis of trivalent lanthanide and uranium diphenylphosphinodiboranates. *Dalton Trans.* **2021**, *50*, 11472–11484.
- (21) Fetrow, T. V.; Zgrabik, J.; Bhowmick, R.; Eckstrom, F. D.; Crull, G.; Vlaisavljevich, B.; Daly, S. R. Quantifying the Influence of Covalent Metal-Ligand Bonding on Differing Reactivity of Trivalent Uranium and Lanthanide Complexes. *Angew. Chem., Int. Ed.* **2022**, *61*, No. e202211145.
- (22) Shannon, R. D. Revised effective ionic radii and systematic studies of interatomic distances in halides and chalcogenides. *Acta Crystallographica, Section A: Crystall Physics, Diffraction, Theoretical and General Crystallography* **1976**, A32, 751–767.
- (23) For related reports investigating the influence of N substituents on the structures of Na and Mg salts of aminodiboranates, the nitrogen congeners of phosphinodiboranates, see: Caroff, C. M.; Bellott, B. J.; Daly, C. I.; Daly, S. R.; Dunbar, A. C.; Mallek, J. L.; Nesbit, M. A.; Girolami, G. S. Sodium Aminodiboranates Na-(H₃BNR₂BH₃): Structural and Spectroscopic Studies of Steric and Electronic Substituent Effects. *Inorg. Chem.* **2022**, *61*, 18412–18423. Caroff, C. M.; Girolami, G. S. Structural and Spectroscopic Studies of Steric and Electronic Substituent Effects in a Series of Magnesium Aminodiboranates Mg[(BH₃)₂NMeR]₂. *Inorg. Chem.* **2023**, *62*, 3116–3122.
- (24) Attempts were made to isolate PDB salts with larger adamantyl (Ad) groups attached to phosphorus, but we were unable to add a second BH₃ group to phosphorus in K(PAd₂BH₃), presumably due to the steric bulk of the adamantyl groups.
- (25) Bowmaker, G. A. Solvent-assisted mechanochemistry. *Chem. Commun.* **2013**, 49, 334–348.
- (26) Eliel, E. L.; Wilen, S. H.; Mander, L. N. Stereochemistry of Organic Compounds; John Wiley & Sons, Inc., 1994.
- (27) Marks, T. J.; Kolb, J. R. Covalent transition metal, lanthanide, and actinide tetrahydroborate complexes. *Chem. Rev.* **1977**, *77*, 263–203
- (28) Ephritikhine, M. Synthesis, Structure, and Reactions of Hydride, Borohydride, and Aluminohydride Compounds of the f-Elements. *Chem. Rev.* **1997**, *97*, 2193–2242.
- (29) Liu, X.; Stern, C. L.; Mirkin, C. A. Chemical Origami: Formation of Flexible 52-Membered Tetranuclear Metallacycles via a Molecular Square Formed from a Hemilabile Ligand. *Organometallics* **2002**, *21*, 1017–1019.
- (30) Pracht, P.; Bohle, F.; Grimme, S. Automated exploration of the low-energy chemical space with fast quantum chemical methods. *Phys. Chem. Chem. Phys.* **2020**, 22, 7169–7192.
- (31) Daly, S. Ř.; Piccoli, P. M. B.; Schultz, A. J.; Todorova, T. K.; Gagliardi, L.; Girolami, G. S. Synthesis and properties of a fifteen-coordinate complex: the thorium aminodiboranate [Th-(H₃BNMe₂BH₃)₄]. *Angew. Chem., Int. Ed.* **2010**, 49, 3379–3381.
- (32) Klamt, A.; Schueuermann, G. COSMO: a new approach to dielectric screening in solvents with explicit expressions for the screening energy and its gradient. *J. Chem. Soc., Perkin Trans.* 2 **1993**, 799–805.
- (33) Daly, S. R. Actinide borohydrides. In The Heaviest Metals: Science and Technology of the Actinides and Beyond; Evans, W. J.,

- Hanusa, T. P., Eds.; Major Reference Works; John Wiley & Sons, Ltd., 2018; pp 319-334.
- (34) Daly, S. R.; Girolami, G. S. Uranium-hydrogen interactions: synthesis and crystal structures of tris(N,N-dimethylaminodiboranato)uranium(III). Chem. Commun. 2010, 46, 407–408.
- (35) Daly, S. R.; Girolami, G. S. Synthesis, characterization, and structures of uranium(III) *N,N*-dimethylaminodiboranates. *Inorg. Chem.* **2010**, 49, 5157–5166.
- (36) Daly, S. R.; Kim, D. Y.; Yang, Y.; Abelson, J. R.; Girolami, G. S. Lanthanide *N*,*N*-dimethylaminodiboranates: highly volatile precursors for the deposition of lanthanide-containing thin films. *J. Am. Chem. Soc.* **2010**, *1*32, 2106–2107.
- (37) Daly, S. R.; Kim, D. Y.; Girolami, G. S. Lanthanide *N,N*-dimethylaminodiboranates as a new class of highly volatile chemical vapor deposition precursors. *Inorg. Chem.* **2012**, *51*, 7050–7065.
- (38) Vlaisavljevich, B.; Miro, P.; Koballa, D.; Todorova, T. K.; Daly, S. R.; Girolami, G. S.; Cramer, C. J.; Gagliardi, L. Volatilities of actinide and lanthanide *N,N*-dimethylaminodiboranate chemical vapor deposition precursors: a DFT study. *J. Phys. Chem. C* **2012**, *116*, 23194–23200.
- (39) Bessen, N. P.; Jackson, J. A.; Jensen, M. P.; Shafer, J. C. Sulfur donating extractants for the separation of trivalent actinides and lanthanides. *Coord. Chem. Rev.* **2020**, 421, 213446.
- (40) Fetrow, T. V.; Grabow, J. P.; Leddy, J.; Daly, S. R. Convenient Syntheses of Trivalent Uranium Halide Starting Materials without Uranium Metal. *Inorg. Chem.* **2021**, *60*, 7593–7601.
- (41) SADABS v.2.03; Bruker AXS Inc.: Madison, WI, 2001.
- (42) Sheldrick, G. M. SHELXT Integrated space-group and crystal-structure determination. *Acta Crystallogr., Sect. A: Foundations and Advances* **2015**, 71, 3–8.
- (43) Sheldrick, G. M. Crystal structure refinement with SHELXL. Acta Crystallogr., Sect. C: Struct. Chem. 2015, 71, 3–8.
- (44) Dolomanov, O. V.; Bourhis, L. J.; Gildea, R. J.; Howard, J. A. K.; Puschmann, H. OLEX2: a complete structure solution, refinement and analysis program. *J. Appl. Crystallogr.* **2009**, *42*, 339–341.
- (45) Macrae, C. F.; Sovago, I.; Cottrell, S. J.; Galek, P. T. A.; McCabe, P.; Pidcock, E.; Platings, M.; Shields, G. P.; Stevens, J. S.; Towler, M.; Wood, P. A. Mercury 4.0: from visualization to analysis, design and prediction. *J. Appl. Crystallogr.* **2020**, *53*, 226–235.
- (46) Perdew, J. P.; Wang, Y. Accurate and simple analytic representation of the electron-gas correlation energy. *Phys. Rev. B, Condens. Matter* **1992**, 45, 13244–13249.
- (47) Tao, J.; Perdew, J. P.; Staroverov, V. N.; Scuseria, G. E. Climbing the density functional ladder: nonempirical meta-generalized gradient approximation designed for molecules and solids. *Phys. Rev. Lett.* **2003**, *91*, 146401–146404.
- (48) Grimme, S.; Antony, J.; Ehrlich, S.; Krieg, H. A consistent and accurate ab initio parametrization of density functional dispersion correction (DFT-D) for the 94 elements H-Pu. *J. Chem. Phys.* **2010**, 132, 154101–154119.
- (49) Eichkorn, K.; Treutler, O.; Ohm, H.; Haeser, M.; Ahlrichs, R. Auxiliary basis sets to approximate Coulomb potentials. [Erratum to document cited in CA123:93649]. *Chem. Phys. Lett.* **1995**, 242, 652–660.
- (50) Eichkorn, K.; Treutler, O.; Ohm, H.; Haser, M.; Ahlrichs, R. Auxiliary basis sets to approximate Coulomb potentials. *Chem. Phys. Lett.* **1995**, 240, 283–290.
- (51) Eichkorn, K.; Weigend, F.; Treutler, O.; Ahlrichs, R. Auxiliary basis sets for main row atoms and transition metals and their use to approximate Coulomb potentials. *Theor. Chem. Acc.* **1997**, *97*, 119–124.
- (52) Kuechle, W.; Dolg, M.; Stoll, H.; Preuss, H. Energy-adjusted pseudopotentials for the actinides. Parameter sets and test calculations for thorium and thorium monoxide. *J. Chem. Phys.* **1994**, *100*, 7535–7542.
- (53) Cao, X.; Dolg, M.; Stoll, H. Valence basis sets for relativistic energy-consistent small-core actinide pseudopotentials. *J. Chem. Phys.* **2003**, *118*, 487–496.

- (54) Dolg, M.; Stoll, H.; Preuss, H. Energy-adjusted ab initio pseudopotentials for the rare earth elements. *J. Chem. Phys.* **1989**, *90*, 1730–1734.
- (55) Weigend, F.; Ahlrichs, R. Balanced basis sets of split valence, triple zeta valence and quadruple zeta valence quality for H to Rn: Design and assessment of accuracy. *Phys. Chem. Chem. Phys.* **2005**, *7*, 3297–3305.
- (56) Dolg, M.; Stoll, H.; Preuss, H. A combination of quasirelativistic pseudopotential and ligand field calculations for lanthanoid compounds. *Theor. Chim. Acta* **1993**, 85, 441–450.
- (57) Cao, X.; Dolg, M. Valence basis sets for relativistic energy-consistent small-core lanthanide pseudopotentials. *J. Chem. Phys.* **2001**, *115*, 7348–7355.
- (58) Weigend, F.; Haser, M.; Patzelt, H.; Ahlrichs, R. RI-MP2: optimized auxiliary basis sets and demonstration of efficiency. *Chem. Phys. Lett.* **1998**, 294, 143–152.
- (59) Ribeiro, R. F.; Marenich, A. V.; Cramer, C. J.; Truhlar, D. G. Use of Solution-Phase Vibrational Frequencies in Continuum Models for the Free Energy of Solvation. *J. Phys. Chem. B* **2011**, *115*, 14556–14562.
- (60) Álvarez-Moreno, M.; de Graaf, C.; López, N.; Maseras, F.; Poblet, J. M.; Bo, C. Managing the Computational Chemistry Big Data Problem: The ioChem-BD Platform. *J. Chem. Inf. Model.* **2015**, 55, 95–103.